General Disclaimer

One or more of the Following Statements may affect this Document

- This document has been reproduced from the best copy furnished by the organizational source. It is being released in the interest of making available as much information as possible.

- This document may contain data, which exceeds the sheet parameters. It was furnished in this condition by the organizational source and is the best copy available.

- This document may contain tone-on-tone or color graphs, charts and/or pictures, which have been reproduced in black and white.

- This document is paginated as submitted by the original source.

- Portions of this document are not fully legible due to the historical nature of some of the material. However, it is the best reproduction available from the original submission.

Analysis of GEOS-3 Altimeter Data and Extraction of Ocean Wave Height and Dominant Wavelength

Edward J. Walsh

March 1979

Analysis of GEOS-3 Altimeter Data and Extraction of Ocean Wave Height and Dominant Wavelength

Edward J. Walsh
Wallops Flight Center
Wallops Island, Virginia

NASA

ANALYSIS OF GEOS-3 ALTIMETER DATA AND EXTRACTION OF
OCEAN WAVE HEIGHT AND DOMINANT WAVELENGTH

Edward J. Walsh
NASA Wallops Flight Center

ABSTRACT

The GEOS-3 satellite radar altimeter has the capability to provide accurate, low noise measurements of the significant wave height (SWH) of ocean waves through their effect on the shape of the return pulse. When the amplitude and timing biases are removed from the GEOS-3 Sample and Hold (S&H) gates, the mean return waveforms can be excellently fitted with a theoretical template which represents the convolution of the radar point target response; the range noise (jitter) in the altimeter tracking loop; the sea surface height distribution; and the antenna pattern as a function of the range to mean sea level. Several techniques of varying complexity to remove the effect of the tracking loop jitter in computing the wave height are considered. They include realigning the S&H gates to their actual positions with respect to mean sea level before averaging; using the observed standard deviation on the altitude measurement to remove the integrated effect of the tracking loop jitter, and using a look-up table to correct for the expected value of range noise. Analysis of skewness in the GEOS return waveform demonstrates the potential of a satellite radar altimeter to determine the dominant wavelength of ocean waves. When the jitter in the GEOS range tracker is large, a significant reduction in range noise reduction can be achieved through reprocessing the data. But when the tracker noise is small only marginal improvement is possible.

INTRODUCTION

The Geodynamics Experimental Ocean Satellite (GEOS-3) was launched on March 30, 1975 into an orbit whose mean altitude is 843 km. The satellite contains a radar altimeter operating at 13.9 GHz which transmits 100 pulses per second towards the subsatellite point. The transmitted pulse of 12.5 ns nominal duration illuminates a pulse-limited spot on the earth's surface whose diameter is 3.6 km on flat terrain. The return waveform is square-law detected and point-sampled by 16 Sample and Hold (S&H) gates of 12.5 ns width

and spaced 6.25 ns apart. One of the major goals of the satellite was to demonstrate that ocean wave heights along the GEOS-3 groundtrack could be extracted from the radar altimeter data. The potential of pulse-limited radar altimeters to measure ocean wave height has been discussed in detail (Barrick, 1972; Miller and Hayne, 1972; Berger, 1972; Walsh, 1974; Brooks and Dooley, 1975), and will not be repeated here. By comparison with in-situ data from waverider buoys and a shipborne wave recorder Walsh et al. (1978) have demonstrated that an airborne pulse-limited altimeter at 3 km altitude can accurately measure wave height.

The author and a number of other GEOS sea state investigators have collaborated on a paper (Fedor et al., 1979) which intercompares our various algorithms, determining the standard deviations and biases of the algorithms using both simulated and actual GEOS data. That paper also compares the GEOS-derived wave heights with data buoy records. Those intercomparisons show that all the algorithms are in good agreement and that the wave height values being produced from GEOS data are accurate. Parsons (1979) has demonstrated on a global basis that GEOS wave height measurements are superior to several other data sources utilized operationally in ship routing and weather forecasting. The purposes of this paper are to examine some GEOS data in detail to demonstrate that the contributions to the mean return waveform are well understood, to examine the techniques for extracting the wave height and skewness of the sea surface height distribution from it, to demonstrate that the skewness may be used to determine the dominant wavelength of the ocean waves, and to gain an appreciation for the promise of the improvements contained in the SEASAT-1 altimeter launched on June 26, 1978.

RADAR ALTIMETER RETURN PULSE SHAPE

The radar mean return pulse is the convolution of the radar system point target response, the jitter (range noise) in the altimeter tracking loop, the sea surface height distribution, and the antenna pattern as a function of the range to mean sea level. Significant wave height (SWH) is defined as the average of the heights of the one-third highest waves in a long sequence of waves observed at a point. For the large spatial averages considered in this paper (70 km) the sea surface height distribution for even a very narrow spectrum would still be nearly Gaussian in which case SWH can be assumed to equal four times the standard deviation of the height distribution (Neumann and Pierson, 1966). To make it easier to assess their relative importance, the widths of the various contributions to the radar mean return signal will be dealt with in terms of effective significant wave heights. For example, four times the standard deviation in meters of the jitter in the range tracking loop will be called the jitter significant wave height, SWH_J.

2

Four times the standard deviation of the rise time of the leading edge of the GEOS-3 return pulse (multiplied by half the speed of light to convert it to radar range) will be called the raw significant wave height, SWH_R. If the antenna pattern is deconvolved (for GEOS-3 this is approximately equal to differentiating the leading edge of the pulse) and if the other contributors to the return pulse are normally distributed then

$$SWH_R{}^2 = SWH_P{}^2 + SWH_J{}^2 + SWH^2 \tag{1}$$

where the subscript P identifies the effective significant wave height associated with the radar point target response (transmitted pulse width and any receiver broadening).

S&H GATE AMPLITUDE AND TIMING BIASES

The 16 GEOS S&H gates have amplitude and timing biases (Walsh, 1979) which should be corrected for to obtain the most accurate wave height results. Figure 1 shows histograms of the outputs of five (1, 6, 8, 10, 16) of the 16 S&H gates. The abscissa quantization
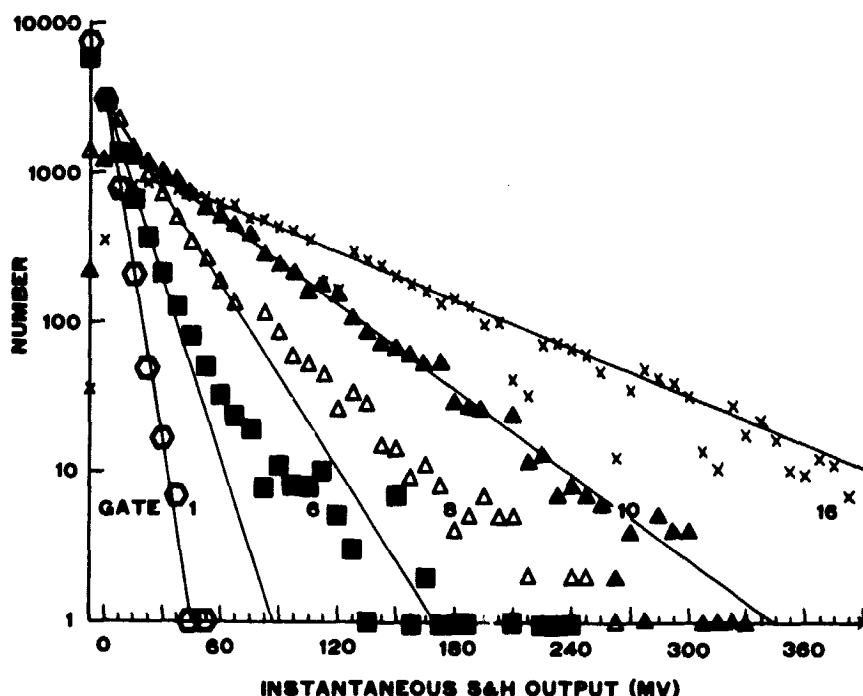

Figure 1.   Histograms of the outputs in mv (proportional to received power) of five (1, 6, 8, 10, 16) of the 16 GEOS Sample-and-Hold (S&H) gates.

3

of 7.5 mv is approximately equal to the quantization of the analog-to-digital (A/D) converters to which the signal voltages (proportional to power) of the S&H gates were applied. Since the ordinate is logarithmic, an exponential distribution of power would result in a straight line. That is the case for the gates sampling the noise ahead of the return pulse (gate 1).

In the region where the return signal is emerging from the noise (gates 6 and 8 in Figure 1) the distribution initially decays exponentially but then decreases more slowly for higher values. This breaking away of the tail probably accounts for the abrupt increase of the fourth order moment as the signal comes out of the noise which has been reported by C. L. Rufenach (1976 Fall AGU Meeting) and suggested as a sensitive indication of the presence of a return signal. When the signal level is high the peak of the distribution is away from the origin but the decay is exponential.

The A/D converter quantization varied somewhat from gate to gate. If the quantization was larger than 7.5 mv then, occasionally, a bin in the histogram might be empty or one quantization level might be split between two adjacent bins. This behavior is in evidence in the histogram for gate 16 in the bins around 120, 210, 262.5 and 315 mv.

Histograms of the outputs of the first five S&H gates are shown in Figure 2 using a much smaller (0.1 mv) bin size. In general, the observations appear as spikes spaced at
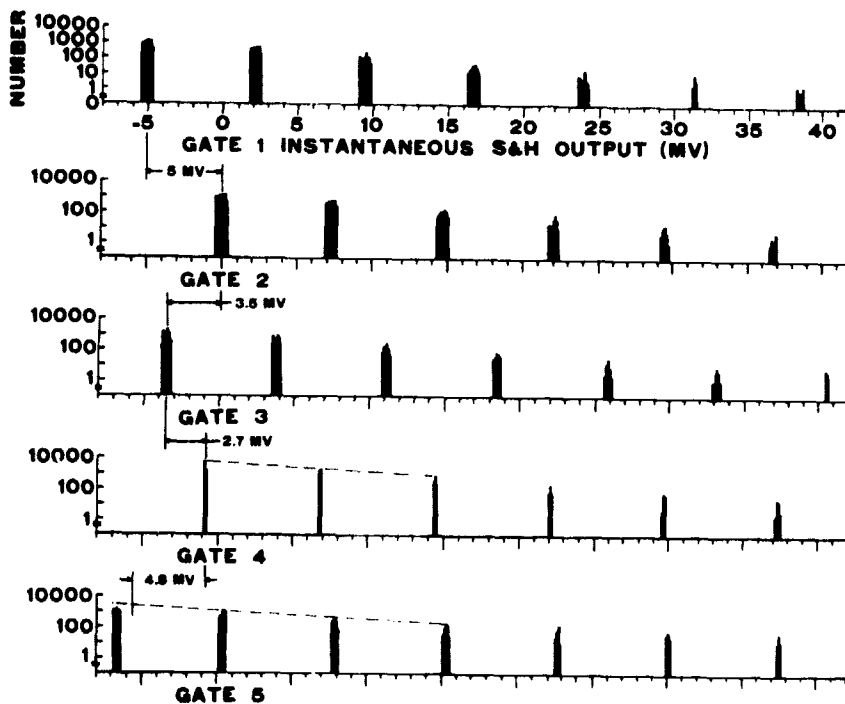

Figure 2. Histograms of the outputs of the first five S&H gates using
a much smaller bin size (0.1 mv) than Figure 1.

4

roughly 7.5 mv intervals. Some of the spikes are narrow (gate 4) while some are rela-
tively broad and exhibit structure of their own (gate 1). The substructure would not have
an important effect on the data since even the broad spikes are narrow with respect to the
7.5 mv spacing. The important consideration is that the various gates have significant
biases with respect to each other.

The lowest entry in the histogram for gate 1 is 5 mv lower than the lowest entry for
gate 2. If the populations of the corresponding spikes in the histograms of gates 1 and 2
are approximately the same then that shift in the distribution would result in the same
magnitude difference in the mean values. Looking at the value of the first spike in each
histogram was the first cut at determining amplitude biases in the gates. In the early
gates a refinement could be made if the populations of the spikes were not the same, such
as gates 4 and 5. If an exponential process were being sampled one could interpolate to
find where the process ended. For gate 5 that would have been 4.8 mv below gate 4 rather
than the 6 mv that would be indicated by the lowest spike in gate 5.

The estimates of the biases were refined using an iterative technique to be described
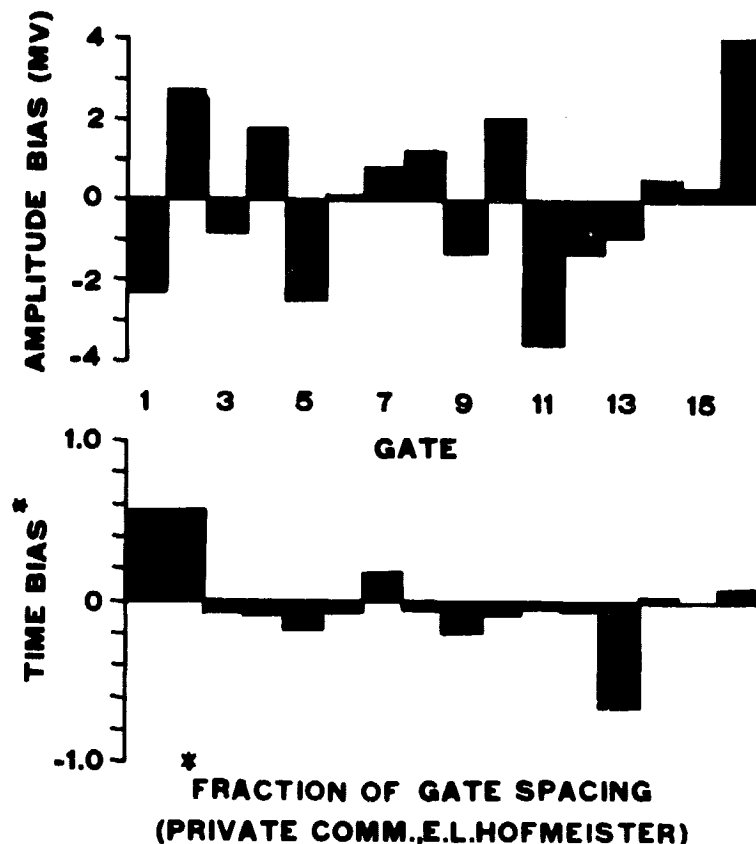later. The results are shown in the top of Figure 3 where the average of the biases for

Figure 3. Amplitude and timing biases for the GEOS altimeter S&H gates.

5

all gates has been arbitrarily set to zero. The bottom of Figure 3 shows the timing biases for the various gates, also zero meaned, which were determined by E. L. Hofmeister of the General Electric Company from prelaunch test data (private communication, 1976). Hofmeister had reported earlier (GEOS-3 PI Meeting/1975) that gate 13 was reading low and was highly correlated with gate 12 and uncorrelated with gate 14. Both effects are explained by the timing bias. The top of Figure 4 shows data points (dots) for three successive 960-pulse averages of GEOS data and the theoretical returns (solid lines) resulting from matching the data with a template formed by convolving a skewed normal distribution (representing the combined effects of surface height distribution, radar point target response, and range noise) with an exponential decay representing the antenna pattern. The amplitude biases are most apparent in the saw tooth pattern of the first five gates.
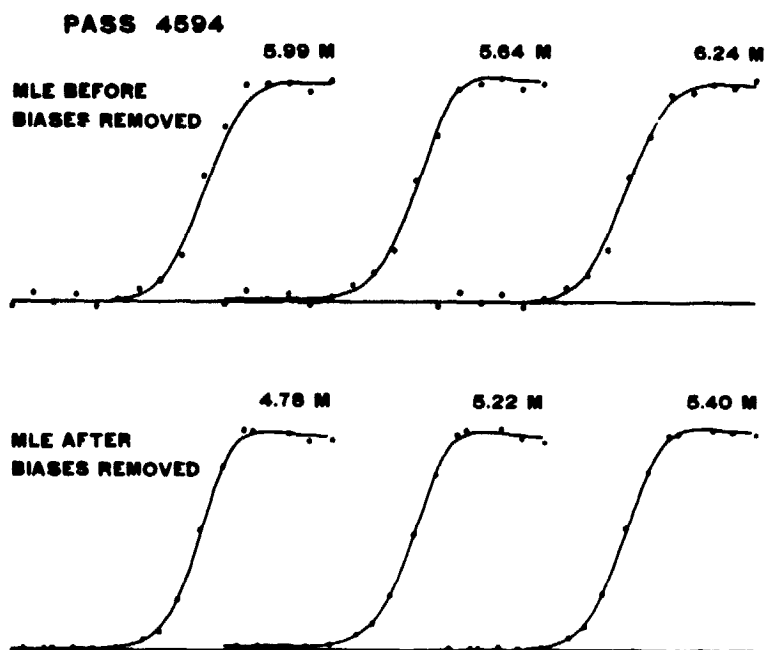

Figure 4.   Data points (dots) for three successive 960-pulse averages of GEOS data and theoretical returns (solid lines) resulting from curve fitting before and after the biases of Figure 3 were removed.

The bottom of Figure 4 shows the same data with the biases removed and the fit redone. The most important timing bias is that gate 13 is closer to gate 12 than it is to gate 14. The fit of the data to the theoretical curves is much improved and the estimates of SWH_R have all lowered. Figure 5 is similar to Figure 4 except that the sea state was higher.
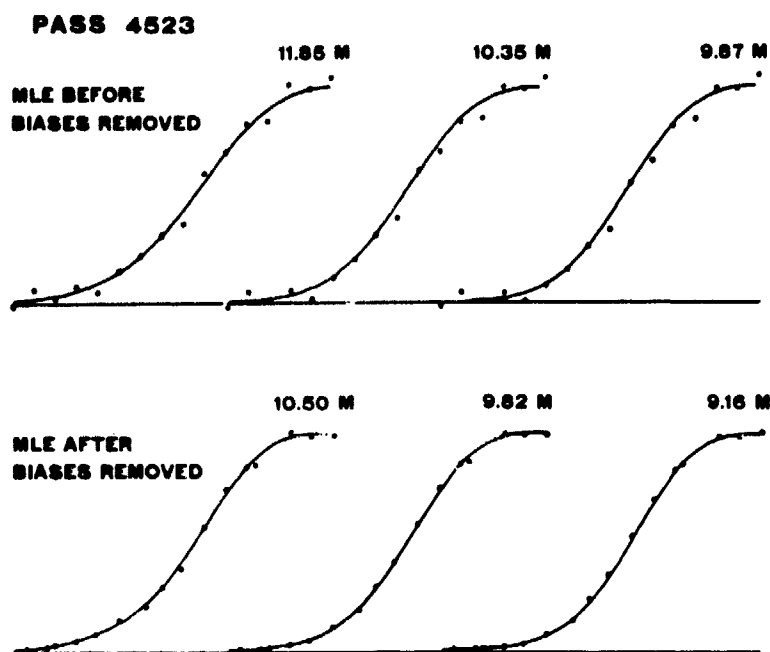
6

Figure 5. Data points (dots) for three successive 960-pulse averages of
GEOS data and theoretical returns (solid lines) resulting from
curve fitting before and after the biases of Figure 3 were
removed.

The GEOS-3 data is recorded in frames containing 320 pulses. Three-frame averages
were used in the data analysis so that the standard deviation in the radar data due to
Rayleigh fluctuations would be only 3.2 percent of the mean value at each point. Refine-
ments to the amplitude biases were made by applying the timing biases and the preliminary
amplitude biases to approximately 30 three-frame averages and determining the template.
If the amplitude biases were correct the data points should fluctuate about the theoreti-
cal returns in a random manner with zero mean. If the mean difference between the data
points and the curves is not zero the amplitude biases were adjusted accordingly and the
procedure repeated. It is apparent from the fit of the data in Figures 4 and 5 that
removing the biases in the GEOS data should produce more accurate results. The timing and
amplitude biases were removed from all the data considered in this paper.

PROCEDURES FOR FITTING DATA WITH THEORETICAL TEMPLATE

The parameters of the theoretical template for the return pulse were varied in an iterative manner and compared with the data to minimize a fit parameter (Walsh et al., 1978). If the fit parameter is the sum of the squares of the residuals of the data to the template then a least-squares (LS) fit is being performed. If the residuals are normalized by the standard deviation observed at each data point before squaring then the fit is a maximum likelihood estimate (MLE). Both procedures were used in fitting the GEOS data. Little difference was found between the two methods for high sea states. At low wave heights the MLE sometimes had trouble converging because relatively small residual errors in the amplitude biases in the noise gates would be highly weighted due to the small standard deviations in those gates. Then the solution would stop before it converged to the correct wave height because the fit parameter would indicate that not much improvement was being made. The biases and the curves in Figures 4 and 5 were derived using MLE estimates but LS estimates were employed in the rest of the paper. J. F. R. Gower (1979) has indicated that the variance of the SWH estimates can be reduced using a hybrid fit where the residuals are normalized by the standard deviation but a limit is placed on how small the standard deviation may become.

TECHNIQUES FOR COMPENSATING FOR RANGE NOISE

Figure 6 shows schematically the ideal and actual positioning of the S&H gates by the tracker. Ideally the gates should be slewed in range smoothly so that gate 10 would always be positioned at the range corresponding to mean sea level (MSL). Actually the tracker does not adjust the range smoothly but jitters the gates back and forth about their ideal positions (shown exaggerated in the figure) so that they are somewhat misaligned. This range noise is generally assumed to be normally distributed. In practice, however, the deviation of the GEOS S&H gates from their ideal position is generally skewed and sometimes can even differ significantly from a skewed-normal distribution.

In the high data rate mode of GEOS when all of the individual pulse-return values of the S&H gates and the range servo error (rse) are available the range jitter effect can be eliminated entirely. Each rse tells the actual change in range of the S&H gates from their previous position and the rse can be integrated to determine the exact spatial positioning of the S&H gates for each pulse. Over a short distance the GEOS-3 satellite altitude variation is very nearly linear. If the integrated rse is detrended by performing a LS fit to a straight line then the residuals are the mispositioning of the gates
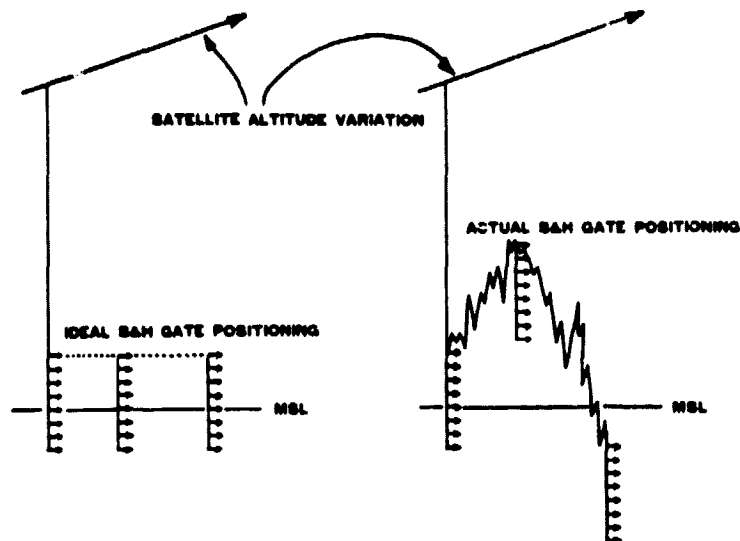
8

Figure 6. Schematic representation of ideal and actual positioning
of GEOS S&H gates by the range tracker.

indicated on the right side of Figure 6. This procedure also removes any linear trend in
MSL due to surface slopes but it should be emphasized that the detrending does not destroy
any information. Any sea surface slope that is present can be recovered if the actual
satellite range rate is known.

The detrending was done over groups of 960 pulses which constitutes three frames of
GEOS data and covers approximately a 70 km ground track. Using only one frame (320 pulses)
was insufficient to insure that the anomalously large deviations (to be discussed later)
sometimes observed in the tracker would not adversely affect the results. The residuals
of the detrended integral of the rse can be used to eliminate range tracker noise by
realigning the individual pulse returns before they are averaged. One can envision on the
right side of Figure 6 that the rse residuals allow the S&H gates to be relabeled to a
primed set of gates that are fixed with respect to MSL. The data in the primed reference
frame would then be free of range tracker noise. If, for example, the gates were posi-
tioned so that S&H gate 10 was actually at the position gate 5 should have been with
respect to MSL, then the data coming in through gate 10 for that pulse would be placed in
the bin corresponding to gate 5 prime for the average data. That essentially turns the
actual tracker shown at the right in Figure 6 into the ideal tracker shown at the left and
eliminates the SWH_J term in (1). For realigned data (1) reduces to

$$SWH_R^2 = SWH_p^2 + SWH^2 \quad \text{(realigned data).} \quad (2)$$

9

Equation (2) is the equation of a circle, as is (1) if the effects of pulse and jitter are combined in a single term such as

$$SWH_{PJ}^2 = SWH_P^2 + SWH_J^2 \ . \tag{3}$$

If both sides of (2) are divided by SWH_R^2 the circle has unit radius as shown in Figure 7. It is apparent that when the SWH is large compared to the pulse (or pulse and jitter in the case of (1)) it is essentially equal to SWH_R. In that region the curve is nearly horizontal so that the error in estimating SWH is essentially equal to the error in estimating SWH_R.
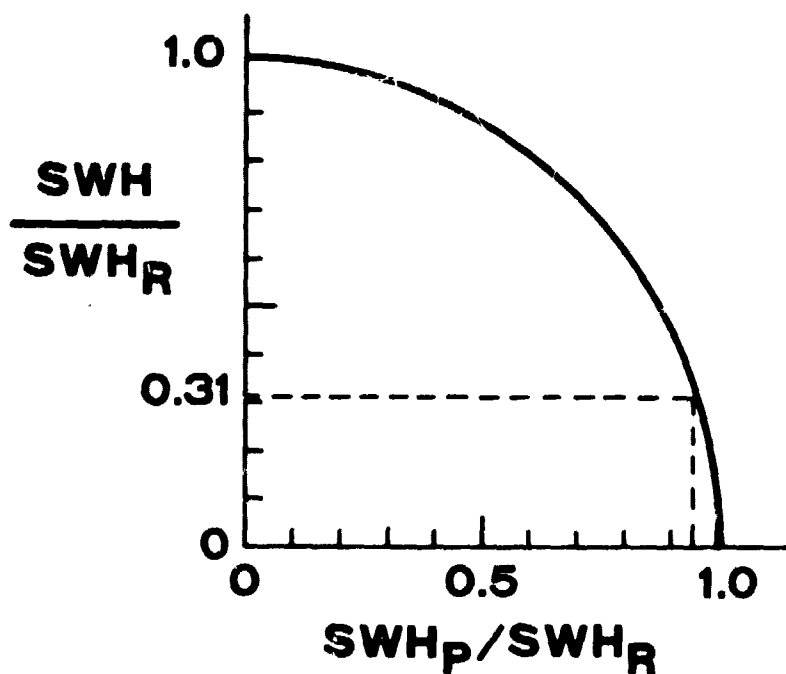

Figure 7. Graphical representation of the relationship between SWH, SWH_P, and SWH_R.

Even in perfectly realigned data the effects of Rayleigh fading in the radar return pulse will cause the measured SWH_R to differ from the ideal. The standard deviation of that measurement depends on a number of things and it is inversely proportional to the square root of the number of pulses averaged. Even a small percentage error in estimating SWH_R produces a large percentage error in SWH when SWH is small compared to the pulse since the curve in Figure 7 is nearly vertical. Figure 7 shows that only a five percent over estimate in SWH_R when the SWH was actually zero would cause the calculated SWH to equal 0.31 SWH_P (1.2 m for GEOS). Similarly, if SWH_R were under estimated by five percent

10

for zero SWH then (2) indicates that the SWH is imaginary and equal in magnitude to 0.31_p. It is apparent that the altimeter pulse width is fundamental in determining the noise in the measurement of low values of SWH. Since the SEASAT-1 altimeter pulse width is nominally a factor of four smaller than the GEOS pulse, its noise level when measuring low wave heights will be correspondingly improved.

Having the SWH computation result in an imaginary number should produce no consternation and introduce no error when one realizes that it is simply a mathematical artifact. Over a series of measurements the measured value of SWH_R will tend to be high as often as it is low, so making the imaginary values of SWH negative is one way of dealing with the problem. Then a series of values of SWH could be filtered to obtain a better estimate of the actual SWH and the positive and negative values of SWH would tend to cancel if the actual SWH were zero. But since the transformations from SWH_R to SWH using (1) or (2) are highly non-linear when SWH is near zero the best procedure to use in filtering the data would be to filter the values of SWH_R to obtain the best estimate of that quantity and then make the transformation to SWH, setting it equal to zero if the computed value were imaginary.

DETERMINATION OF SWH

Figure 8 shows dashed curves representing the raw significant wave height, SWH_R, and the range jitter, SWH_J, obtained from non-overlapping three-frame averages of GEOS data. The effective significant wave height of the radar point target response, SWH_p, is constant at 3.81 m and will not be shown on the figures. Computing SWH using (1) results in the data points (squares and diamonds) which indicate a fairly constant SWH around 3.5 m except for the average of frames 67, 68, 69 where it is indicated as zero. At that point (1) indicated that SWH^2 was equal to -13.9. In this instance the imaginary SWH value is not due to Rayleigh fluctuations in the return pulse but is caused by over estimating SWH_J because the range jitter is not normally distributed in that region. It can be eliminated by realigning the individual return pulses before averaging so SWH is determined from (2) instead of trying to compensate for the integrated effect of the tracker misalignment in the averaged data using (1). The SWH values determined using the realigned data are shown by the solid curve in Figure 8. The circle is the SWH measured by a 3 ns pulse-limited radar altimeter (Hughes Aircraft Company, 1976) from a NASA WFC C-54 aircraft during a simultaneous GEOS underflight at 3 km altitude. The two methods of extracting SWH from GEOS data are in reasonable agreement except where the SWH value was anomalously low using the first technique.

The range noise for the 12 frames of data corresponding to the four diamonds in

11

Figure 8 is shown at the top of Figure 9. The residuals of the detrended integral of the rse are shown at the top of the figure. At the bottom of the figure are shown histograms of the deviations of the S&H gate positions from the ideal position for each of the four three-frame averages. The abscissa and ordinate of each histogram have been normalized appropriately using the standard deviation observed in the data to correspond to the normal distributions indicated by the dots. The first and second histograms are very nearly normally distributed with some skewness and the fourth histogram is not too far off. But the third distribution is non-normal and considerably more narrow than is indicated by its standard deviation. The reason for the anomalously low SWH value in Figure 8 was because the high value of SWH_J was not a true indication of the width of the distribution. The large excursion is an example of the tracker anomalies referred to earlier and is not caused by a variation in the level of the sea surface.

Because a relatively small number of large residuals can cause too large a value of SWH_J there is a tendency for the values of SWH produced by (1) to be lower than those obtained using (2) even when the effect is not striking as it was in Figure 8. Figure 10 shows a pass where no imaginery SWH values were produced by (1) but that algorithm tended to produce lower values than the realignment process. The higher values produced by (2) are in better agreement with the value of SWH measured from 3 km altitude by the Naval Research Laboratory radar altimeter (also on the NASA aircraft, see Walsh et al. (1978) for an analysis of its measurement capabilities). Figure 11 shows the range noise and histograms for the four three-frame averages indicated by the diamonds on Figure 10. The second of the four histograms is the closest to a skewed-normal distribution and yet the results of (1) and (2) differ by 1.5 m.

Figure 12 shows a third case where there is both good and poor agreement between the two techniques. Since SWH is a measure of how much energy is contained in the sea surface wave pattern it generally would be expected to be a smoothly varying function when averaged over the many ocean wavelengths that would be contained in the 70 km distance traveled during a three-frame average. One would expect that most of the fluctuation in SWH_R from one three-frame average to another would be caused by, and in phase with, fluctuations in range noise. This behavior is in evidence in all three of the figures, 8, 10, and 12, but a particularly good example appears in the Figure 12 in the region from frame ₋2 to frame 45. There is a saw-tooth variation in both SWH_R and SWH_J but the SWH determined from (1) shows a gradual trend. It is not surprising that the agreement between SWH determined by (1) and (2) is good in that region.

On the other hand, there is also a saw-tooth pattern in evidence in the region from frame 61 to frame 75. Although the SWH_R and SWH_J patterns are in phase, the high values of SWH_J are anomalously high due to those distributions of rse residuals being non-normal as evidenced by the histograms in Figure 13. The result is that the SWH calculated from (1) decreased sharply when SWH_R increased at frames 64 and 70.
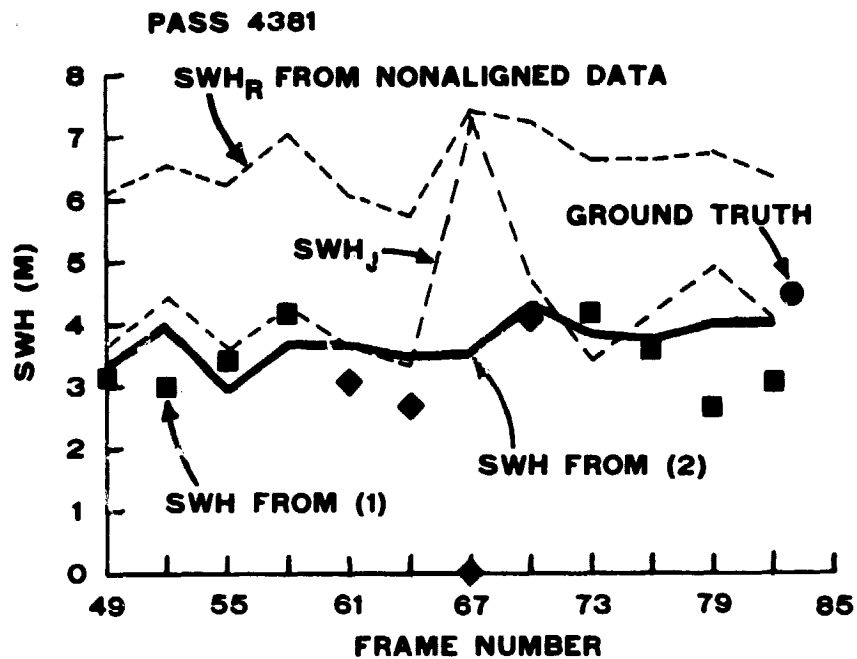
12

PASS 4381

Figure 8. Plots of SWH_R, SWH_J and SWH for non-overlapping three-frame averages of GEOS data for pass 4381.
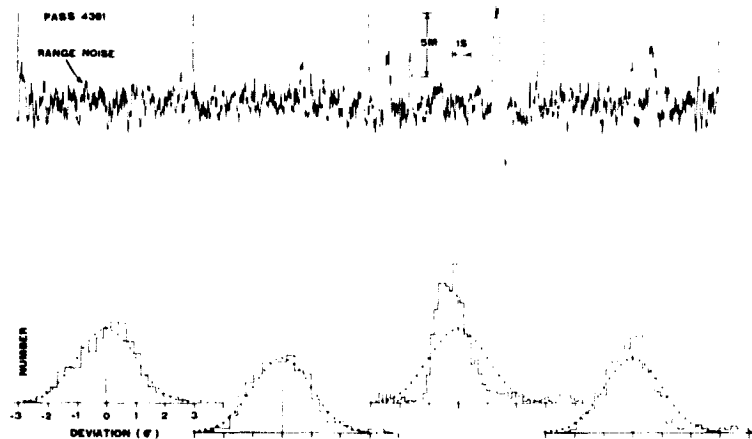

Figure 9. A plot of the residuals of the detrended integral of the range servo error and histograms of the residuals for the data corresponding to the diamonds in Figure 8.

Figure 10. Plots of SWH_R, SWH_J and SWH for non-overlapping three-frame averages of GEOS data for pass 4523.

Figure 11. A plot of the residuals of the detrended integral of the range servo error and histograms of the residuals for the data corresponding to the diamonds in Figure 10.
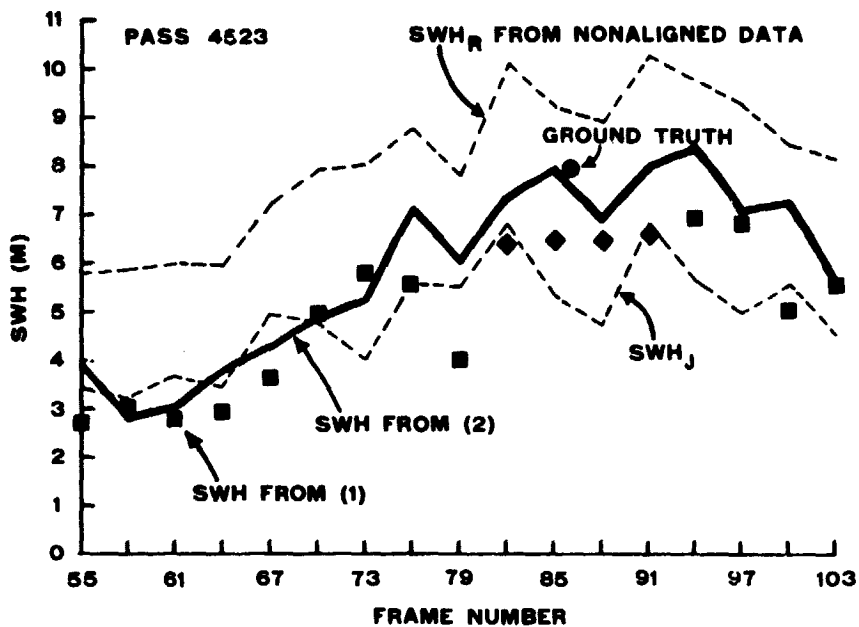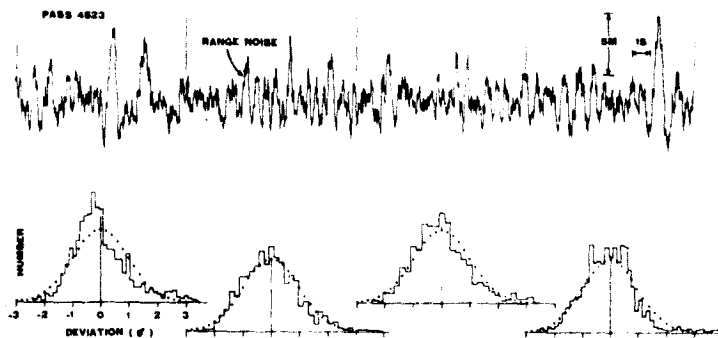
14

Figure 12.   Plots of SWH_R, SWH_J and SWH for non-overlapping three-frame averages of GEOS data for pass 4481.

Figure 13.   A plot of the residuals of the detrended integral of the range servo error and histograms of the residuals for the data corresponding to the diamonds in Figure 12.
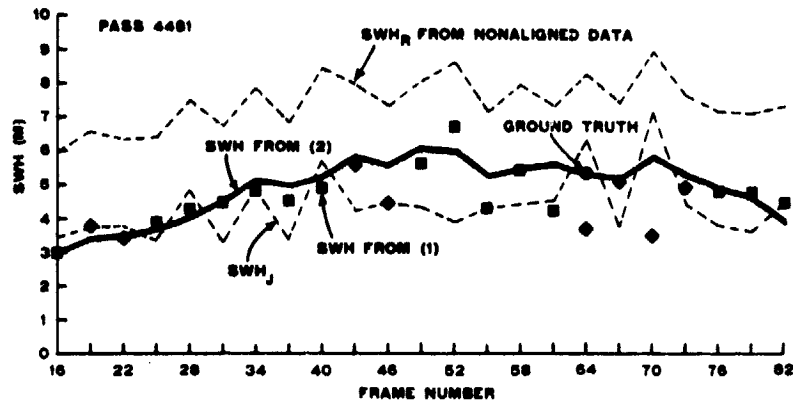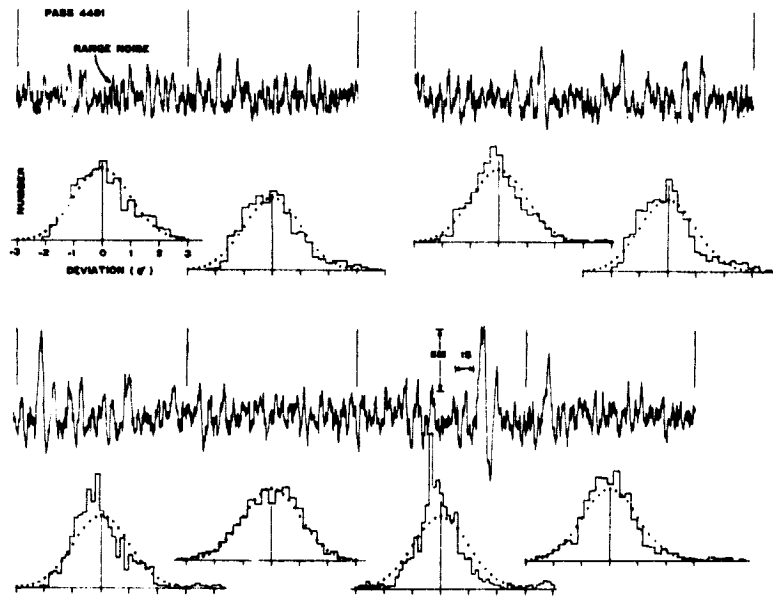
15

It is also unrealistic from a consideration of the hardware that SWH would decrease sharply when SWH_R increases. The range tracker bandwidth increases as the SWH decreases and the faster response should decrease the range noise. A decrease in the actual SWH should decrease both SWH_J and SWH_R, not increase them. The range noise distributions at frames 67 and 73 are closer to being normal and the agreement is better between the values of SWH determined from (1) and (2).

During the preprocessing of the GEOS data by NASA WFC the altitude standard deviation, σ_H, is computed for each frame and placed on the data tapes before they are disseminated. Figure 14 is a scatter plot, versus SWH_J, of the altitude standard deviation multiplied by four to convert it to an effective wave height. Because SWH_J was calculated on a three-frame basis, the square root of the mean of the squares of the three σ_H values was used for the comparison. The slope of the straight line through the data points is 45° but the SWH_J intercept is 0.5 m which indicates that the two quantities typically differ by 0.5 m. If all the values of rse were not available (low data rate) or if one didn't wish to take the computer time to integrate the rse and detrend it, the values of σ_H could be used to determine a value of SWH_J for use in (1).
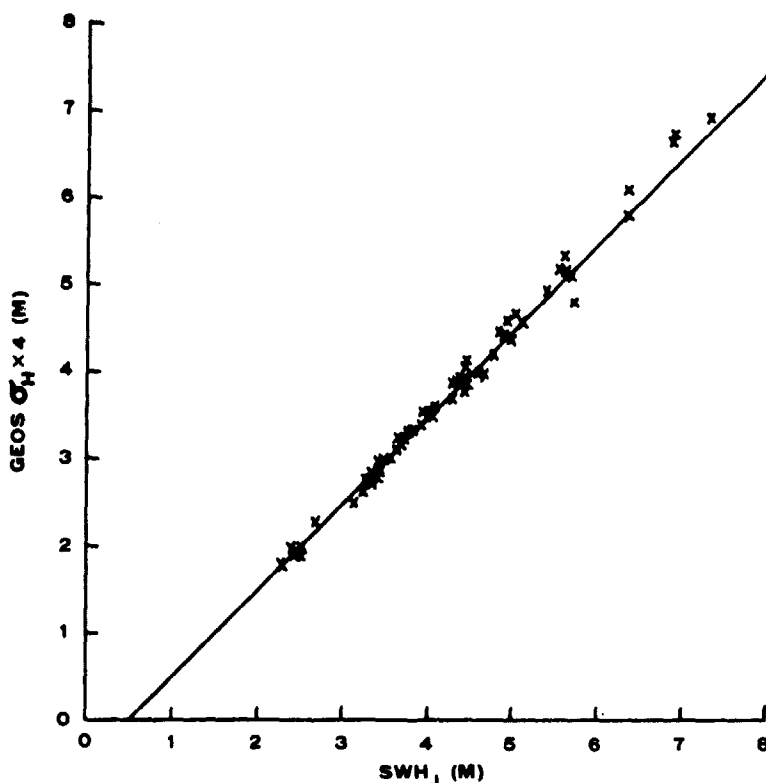

Figure 14. Scatter plot of altitude standard deviation computed by NASA WFC during preprocessing of GEOS data versus SWH_J. The straight line is at a 45° angle.

16

Hofmeister et al. (1976) have done a detailed analysis of the GEOS range tracker. But a very simple analysis will suffice here to put the GEOS data in perspective. To first order one would expect the tracking jitter to be inversely proportional to the mean slope of the leading edge of the return pulse. Another way of saying the same thing is that it should be proportional to the rise time of the return pulse. But that implies

$$SWH_J = K \sqrt{SWH_p^2 + SWH^2} \qquad (4)$$

where K is a constant which is equal to the ratio SWH_J/SWH_p when SWH is zero.

Figure 15 is a scatter plot of range jitter versus the SWH determined from realigned data using (2). The open circles indicate points associated with tracker anomalies. The dashed curve is a plot of (4) for K = .6955. Figure 16 is a scatter plot of SWH determined from realigned data versus SWH_R from non-aligned data. The dashed curve is a plot the equation resulting from substituting (4) into (1).

$$SWH_R^2 = (1 + K^2) (SWH_p^2 + SWH^2) \qquad (5)$$

The curve is in fairly good agreement with the data points but a better fit to the data could be made using a curve whose slope was slightly steeper at the high end.
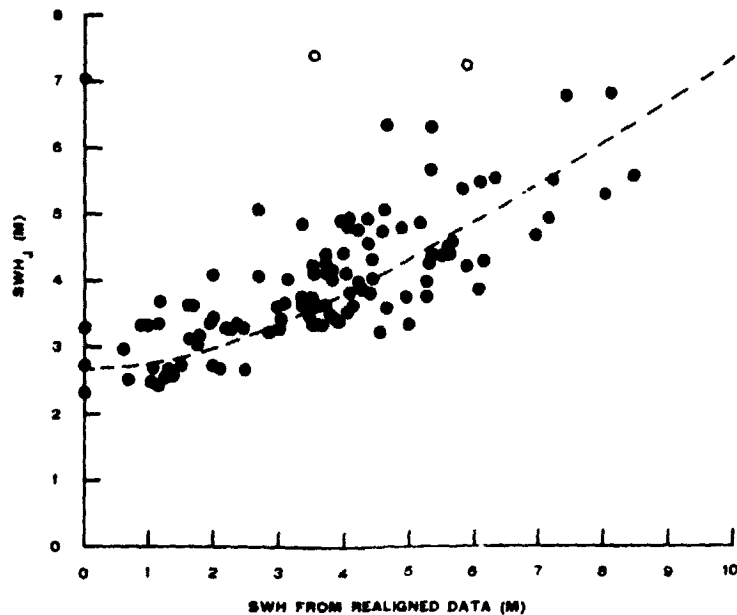

Figure 15. Scatter plot of range jitter versus SWH determined from realigned data. The open circles indicate points associated with tracker anomalies. The dashed curve is a theoretical result assuming tracker noise is proportional to rise time of return pulse.

17

The most accurate technique of extracting SWH from GEOS-3 data would be to do the realignment and use (2). When that approach is not possible (low data rate) or when the computer time to do the realignment is too costly then the best procedure would probably be to use a look-up table to go directly from SWH_R to SWH rather than use (1). The look-up table could be generated using a curve similar to the one shown in Figure 16 but one which had been least-squares fitted to the data points. Then SWH_J would not have to be considered. Even regions of non-normally distributed range noise would cause little difficulty since they affect SWH_J much more than they do SWH_R.
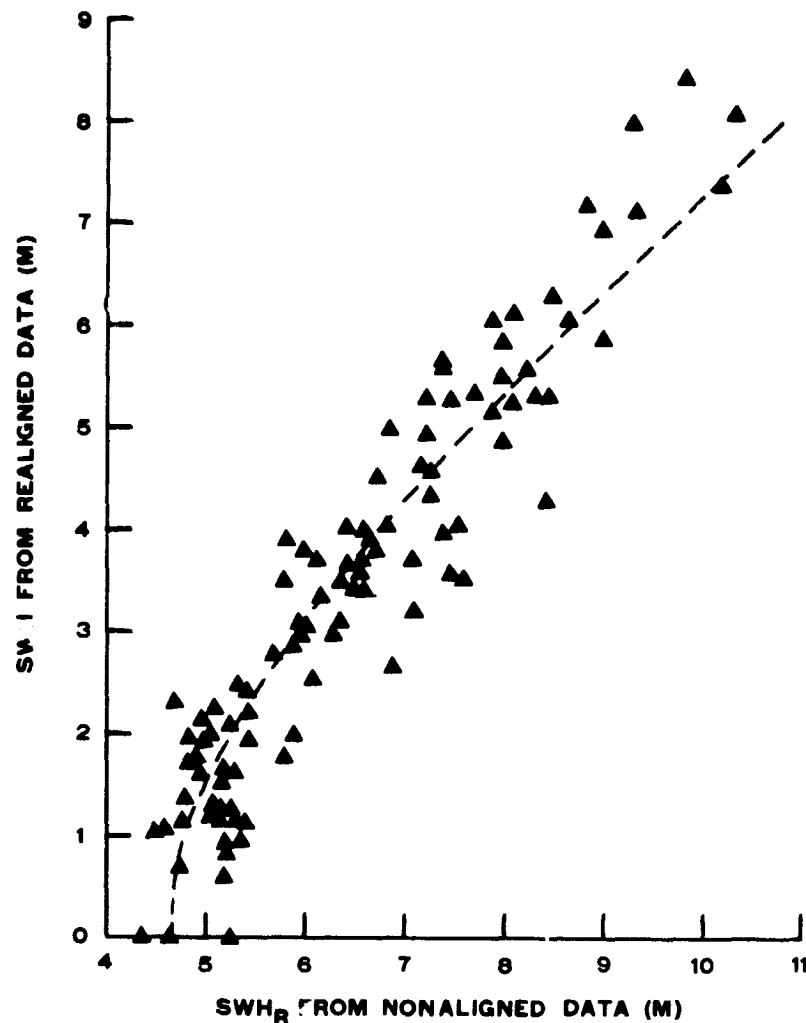

Figure 16. Scatter plot of SWH determined from realigned data versus SWH_R from nonaligned data. The dashed curve is the theoretical result expected using the dashed curve from Figure 15.

18

Figures 8, 10, and 12 show values of SWH_J reaching 5 to 7 m. Under similar conditions the value of SWH_J for the SEASAT altimeter should not exceed 0.40 m. That, combined with the low value of SWH_p for SEASAT, indicates that SWH will essentially equal SWH_R for all but the lowest wave heights. And they should readily be determined from a look-up table.

MEASUREMENT OF SKEWNESS OF SEA SURFACE HEIGHT DISTRIBUTION

As discussed earlier, the theoretical template which was fit to the GEOS data contained skewness as a parameter. The skewness determined from the template would be the raw skewness, λ_R, associated with SWH_R. Prof. W. J. Pierson has shown (private communication, 1977) that if each of the contributors to SWH_R is a skewed-normal distribution then λ_R is equal to

$$\lambda_R = \lambda \left(\frac{SWH}{SWH_R}\right)^3 + \lambda_p \left(\frac{SWH_p}{SWH_R}\right)^3 + \lambda_J \left(\frac{SWH_J}{SWH_R}\right)^3 \tag{6}$$

where λ, λ_p, and λ_J are the skewness values associated with the surface height distribution, the radar point target response, and the range noise.

As is apparent in the histogram of Figure 9, 11, and 13, the GEOS range noise is generally highly skewed and sometimes non-normally distributed. The mean value of λ_J is 0.5 and the standard deviation is 0.4. Figure 15 shows that SWH_J is roughly the same magnitude as SWH for high wave heights and considerably larger than SWH for low wave heights. So range noise would make it very difficult to use (6) to extract λ from GEOS data. If realigned data is used then (6) reduces to (7).

$$\lambda_R = \lambda \left(\frac{SWH}{SWH_R}\right)^3 + \lambda_p \left(\frac{SWH_p}{SWH_R}\right)^3 \tag{7}$$

Figure 17 shows some results of a simulation performed by the author and described in Fedor et al. (1978). Rayleigh fluctuations were added to theoretical GEOS mean return wave forms for realigned data of known SWH_R and λ_R simulate returns corresponding to averages of various numbers of pulses. Estimates of the various parameters were made using the simulated data and their means and standard deviations were computed. The standard deviation of λ_R was approximately independent of the mean value and varied inversely as the square root of the number of pulses averaged. Figure 17 shows that estimation of skewness is a noisy process for one-frame averages of GEOS data, especially
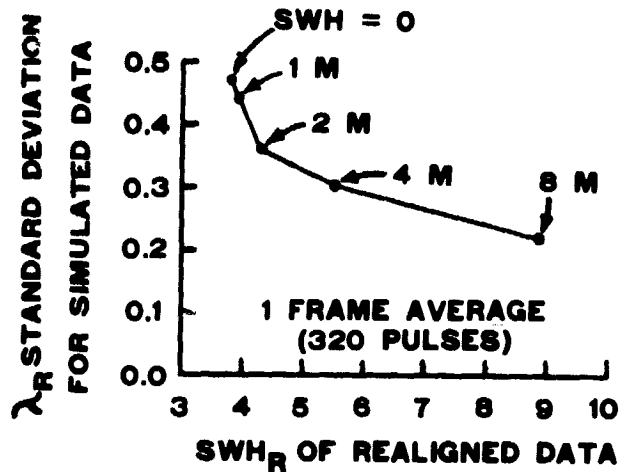
19

Figure 17. Expected standard deviation of λ_R estimate derived from stimulated realigned GEOS data.

for the lower values of SWH.

To determine the on-orbit value of skewness for the radar point target response GEOS-3 data was processed for three passes (4590, 5443, 6629) which same passed by closest approach (< 30 km) a NOAA National Data Buoy (EB-15) indicating that the wave field was low swell (wind $\leq$ 2.4 m/s, SWH $\leq$ 0.7 m, wave period > 5 seconds). The GEOS data itself indicated that there was a large area in the vicinity of the buoy on each of the passes where the wave height was very low.

The mean value of λ_R for the three-frame averages of realigned GEOS data was 0.46 for the segments used from the three passes. The standard deviation on those λ_R estimates was 0.26 which agrees with the simulation results since it is just $\sqrt{3}$ times smaller than the value indicated in Figure 17 for the 0 to 1 m range of SWH for one-frame averages.

The theory discussed in the next section indicates that λ would be approximately 0.1 or less for the conditions described by the buoy. The small ratio of SWH/SWH$_R$ and the cubic weighting in (7) make the contribution of λ to λ_R negligible under those conditions and the value of λ_p can be calculated to be 0.48.

Equation (7) can be rearranged to form

$$\lambda = \lambda_R \left(\frac{SWH_R}{\overline{SWH}} \right)^3 - \lambda_p \left(\frac{SWH_p}{\overline{SWH}} \right)^3 \tag{8}$$

When SWH is large compared to SWH$_p$ then it is approximately equal to λ_R. But when SWH is small compared to SWH$_p$ then λ is, in general, the difference of two relatively large terms and would be difficult to determine accurately.

20

DETERMINATION OF DOMINANT WAVELENGTH

In the recent theoretical study quantitatively confirmed by laboratory and field data, Huang and Long (1979) determined that the skewness of the height distribution of waves is proportional to the significant slope, $\S$. This significant slope was defined as the ratio of rms wave height to dominant wavelength where the dominant wavelength was determined by the maximum of the wave height frequency spectrum. Their theoretical result was

$$\lambda = 8\pi \S. \qquad (9)$$

Data from the passes shown in Figures 10 and 12 provide an excellent opportunity to examine the possibility of using their result to determine dominant wavelength. The wave height was essentially all sea in Figure 10 at the position of the ground truth data point and all swell at the same position in Figure 12.

For the position of the NASA ground truth aircraft along pass 4523 (Figure 10) the hindcast indicated that the wind was 20 m/s at 240° and the wind-driven sea had an 8 m SWH with an eight second period while the swell was only 1 m with a 14 second period. The hindcast SWH seems to be accurate since the composite SWH would be 8 m which is in agreement with both the GEOS SWH and the aircraft measured SWH. Two independent estimates of the wind were obtained from the aircraft (Robert Mennella, private communication, 1977). Taking 0.8 times the wind velocity measured by the aircraft at 150 m altitude resulted in a surface wind estimate of 22 m/s at 229°. Estimating the magnitude of the surface wind using the NRL radar in the Wind-Wave-Radar (WWR) mode (Hammond et al., 1977) resulted in 18 m/s.

For the position of the aircraft along pass 4481 (Figure 12) the hindcast indicated that the wind was 5 m/s at 260° and the wind-driven sea was only 0.5 m with three second period while the swell was 6 m with ten second period. The hindcast also seems fairly accurate in this case since the GEOS and aircraft measured SWH values were 5.4 m. The wind estimate using 0.8 times the aircraft-measured wind velocity at 150 m resulted in 9 m/s at 281° and the WWR estimate of the surface wind magnitude was 7.6 m/s. Since the highest SWH that could be expected to be produced by an 8 m/s wind would still be less than 1.5 m it is reasonable to assume that the waves were essentially all swell.

Figure 18 is a plot of λ for passes 4523 and 4481 versus distance from the ground truth data points. The values of λ were determined from nine-frame averages of GEOS data (210 km ground track) to improve the accuracy of the measurement. The center of the nine-frame average was shifted three frames at a time (70 km) so that adjacent data points on the plot were obtained from average data which had six frames in common. Both plots show
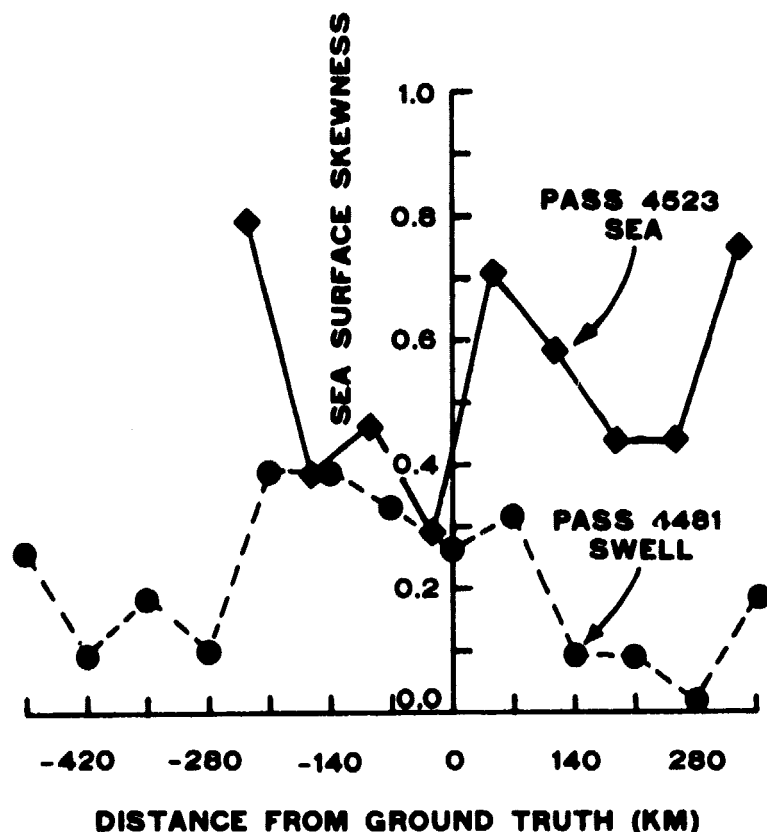
Figure 18. Variation of sea surface skewness as determined from GEOS data for wind-driven sea and swell conditions. The mean values of λ over the data points were 0.48 for the wind-driven sea and 0.21 for the swell.

a significant variation in skewness, but the mean of the values for the wind-driven sea (pass 4523) is 0.54 which is significantly higher than the 0.21 mean value for the swell (pass 4481).

Figure 19 is a plot of (7) where two axes have been used on the abscissa. One axis is in terms of § and one is in terms of the ratio of dominant wavelength to SWH, which is 0.25 times the reciprocal of §. Data from passes 4523 and 4481 are shown on the figure with the vertical positions of the diamond and circle indicating the mean of the respective skewness values shown in Figure 18. The error bars on the mean values are the standard deviations of the Figure 18 data points reduced by the square root of one third the number of points averaged to account for the correlation caused by the overlap in the averages. The horizontal position of the diamond is the ratio of the wavelength indicated by the hindcast (96 m wavelength corresponding to an eight second period) to the 8 m SWH determined by GEOS (which agreed with the hindcast and aircraft data). The horizontal
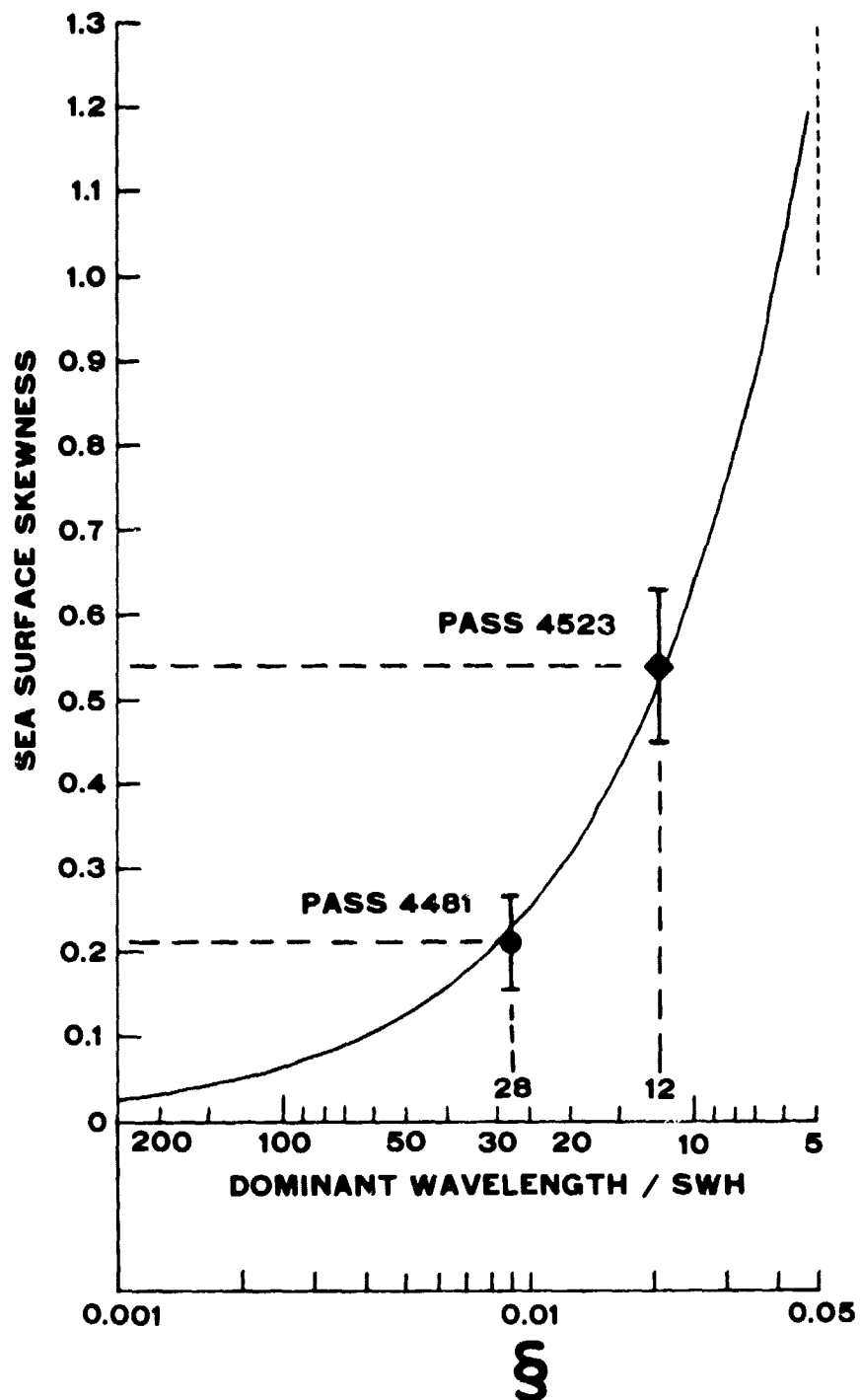
22

Figure 19. Theoretical curve from Huang and Long (1979) showing the relationship between sea surface skewness and dominant wavelength and GEOS-3 data points.

position of the circle uses the 150 m wavelength corresponding to the ten second hindcast period and the 5.4 m GEOS SWH (which agreed with the aircraft data but was slightly lower than the 6 m hindcast SWH).

Figure 19 indicates that an altimeter could be used to determine the dominant wavelength of the ocean waves. The SWH and skewness can be determined from the returned pulse shape. Then SWH can be multiplied by the ratio of dominant wavelength to SWH determined from Figure 19 and the skewness. Two data points are by no means definitive but they do demonstrate the potential. An extensive analysis of satellite radar altimeter data and comparison with surface truth needs to be done to firmly establish this remote sensing technique. The pulse repetition rate of the SEASAT-1 altimeter is ten times higher than GEOS-3, the pulse width is four times smaller, the data point spacing on the return waveform is twice as dense and the SWH_J is below 0.4 m. Therefore, for SEASAT-1 λ should nearly equal λ_R, the spatial sampling of λ on the ocean will be higher and the noise level on the measurement will be lower.

NOISE REDUCTION IN RANGE MEASUREMENT

In addition to SWH_R and λ_R, another parameter that is determined in the process of fitting the theoretical return to the data is the arrival time (epoch) of the return pulse. The left side of Figure 20 shows that when the GEOS raw range noise is high then realigning the pulses and determining the epoch for 30-pulse averages will significantly reduce the noise in the range measurement compared to simply averaging the range data. However, if the GEOS tracker noise is in its typical range, then the amount of improvement to be gained using the more complex technique is small (right side of Figure 20). This same conclusion was arrived at by Dooley et al. (1979) after a more complex analysis. It should be noted that range tracker anomalies such as the one seen in Figure 9 completely disappear when the pulses are realigned and retracked. That is the best evidence that they are not indications of surface elevation changes. Realigning pulses should never be necessary on SEASAT-1 altimeter data since the range noise should generally be below 10 cm.

CONCLUSIONS

The contributions to the mean return waveform of a pulse-limited radar altimeter are well understood. The GEOS-3 satellite radar altimeter is providing accurate, low noise

GEOS-3 RANGE NOISE

PASS 4632 FRAMES 62,63,64   FRAMES 65,66,67

RAW DATA
σ = 172 CM   σ = 98 CM

AVG. OF
30 DATA POINTS
σ = 151 CM   σ = 49 CM

REALIGNED
30-PULSE AVG.
σ = 58 CM   σ = 43 CM
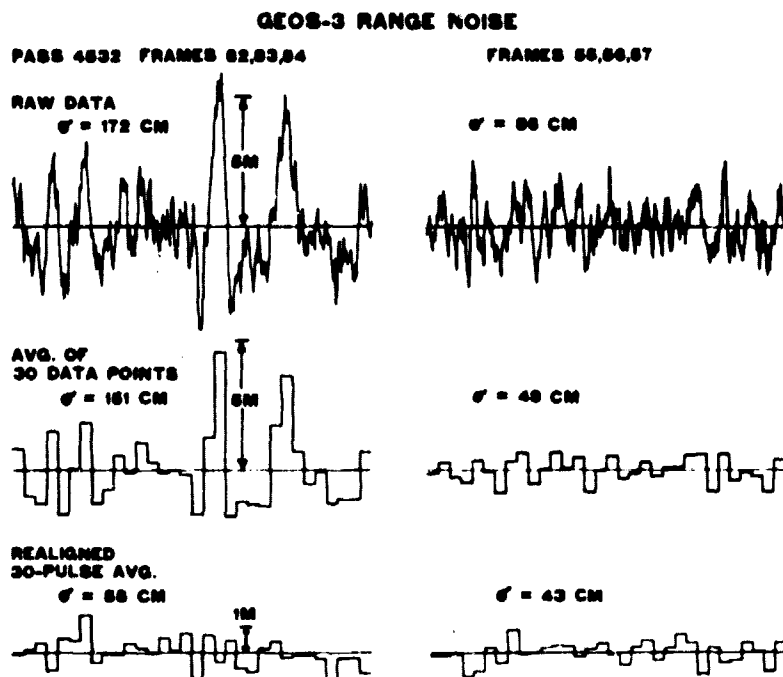
Figure 20.   GEOS tracker range noise and range noise resulting from
             averaging range data points versus realigning and retracking
             the return pulses.

measurements of the significant wave height of ocean waves. Analysis of skewness in the
GEOS return waveform demonstrates the potential of a satellite radar altimeter to deter-
mine the dominant wavelength of ocean waves. When the jitter in the GEOS range tracker is
large, a significant reduction in range noise reduction can be achieved through reproces-
sing the data. But when the tracker noise is small only marginal improvement is possible.
The SEASAT-1 altimeter should produce even more accurate SWH and dominant wavelength
values with greater spatial resolution than GEOS-3.

ACKNOWLEDGMENTS

REFERENCES

1. Barrick, D. E.: 1972, "Remote Sensing of Sea State by Radar," in Remote Sensing of the Troposphere, edited by V. E. Derr, U.S. Government Printing Office, Washington, D.C. 20402, 12-34, 12-41.

2. Berger, T.: 1972, "Satellite Altimetry Using Ocean Backscatter," IEEE Trans. Antennas Propagation. AP-20, 295-309.

3. Brooks, L. W., and Dooley, R. P.: 1975, "Technical Guidance and Analytic Services in Support of SEASAT-A," NASA Contractor Report CR-141399, NASA Wallops Flight Center, Wallops Island, VA 23337, N75-20803, pp. I-3-11 to I-3-33.

4. Dooley, R. P., Brooks, L. W., and Khoury, E. N.: 1979, "Optimization of Satellite Altimeter and Wave Height Measurements," NASA Contractor Report CR-156850, NASA Wallops Flight Center, Wallops Island, VA 23337.

5. Fedor, L. S., Godbey, T. W., Gower, J. F. R., Guptill, R., Hayne, G. S., Rufenach, C. L., and Walsh, E. J.: 1979, "Satellite Altimeter Measurements of Sea State - An Algorithm Comparison," JGR, 84.

6. Gower, J. F. R.: 1979, "Measurements of Ocean Surface Wave Height Using GEOS-3 Satellite Radar Altimeter Data," Remote Sensing of Environment, in press.

7. Hammond, D. L., Mennella, R. A., Walsh, E. J.: 1977, "Short Pulse Radar Used to Measure Sea Surface Wind Speed and SWH," IEEE Transactions Antennas Propagation, AP-25, No. 1, 61-67.

8. Hofmeister, E. L., Keeney, B. N., Godbey, T. W., and Berg, R. J.: 1976, "Data User's Handbook and Design Error Analysis, GEOS-C Radar Altimeter, Volume I," Prepared by General Electric Company, Utica, New York 13503, under contract numbers NASA NAS6-2619 and APL 372165.

9. Huang, N. E., and Long, S. R.: 1979, "A Study of the Wave Height Probability Distribution and Statistics of Wind Generated Waves," submitted for publication, Journal of Fluid Mechanics.

10. Hughes Aircraft Company: 1976, Final Report of the Advanced Application Flight Experiment Breadboard Pulse Compression Radar Altimeter Program, NASA CR-141411, NASA Wallops Flight Center, Wallops Island, VA 23337.

11. Miller, L. S., and Hayne, G. S.: 1972, "Characteristics of Ocean-Reflected Short Radar Pulses with Application to Altimetry and Surface Roughness Determination," Sea Surface Topography from Space, vol. 1, NOAA Tech. Rep. ERL 228-AOML 7, U.S. Government Printing Office, Washington, DC 20402, N73-15381, 12-1 to 12-32.

12. Neumann, G., and Pierson, W. J.: 1966, "Principles of Physical Oceanography," Prentice-Hall, Englewood Cliffs, NJ, 351.

13. Parsons, C. L.: 1979, "GEOS-3 Wave Height Measurements: An Assessment During High Sea State Conditions in the North Atlantic," JGR, 84.

14. Walsh, E. J.: 1974, "Analysis of Experimental NRL Radar Altimeter Data," Radio Science, 9, No. 8, 9, 711-722.

15. Walsh, E. J., Uliana, E. A. and Yaplee, B. S.: 1978, "Ocean Wave Heights Measured by a High Resolution Pulse-Limited Radar Altimeter," Boundary-Layer Meteorology, 13, 263-276.